Manuscript prepared for Geosci. Model Dev. Discuss.
with version 2014/07/29 7.12 Copernicus papers of the LaTeX class copernicus.cls.
Date: 31 July 2015

On the use of Schwarz–Christoffel conformal mappings to the grid generation for global ocean models

S. Xu[1], **B. Wang**[1,2], **and J. Liu**[3]

[1]Ministry of Education Key Laboratory for Earth System Modeling, Center for Earth System Science (CESS), Tsinghua University, Beijing, China
[2]State Key Laboratory of Numerical Modeling for Atmospheric Sciences and Geophysical Fluid Dynamics (LASG), Institute of Atmospheric Physics, Chinese Academy of Sciences, Beijing, China
[3]Department of Atmospheric and Environmental Sciences, University at Albany, State University of New York, Albany, NY 12222, USA

Correspondence to: S. Xu (xusm@tsinghua.edu.cn)

Abstract

In this article we propose two conformal mapping based grid generation algorithms for global ocean general circulation models. Contrary to conventional, analytical forms based dipolar or tripolar grids, these new methods are based on Schwarz-Christoffel conformal mappings which map areas of irregular boundaries to those with regular boundaries (i.e., disks, slits, etc.). They not only relocate the North Pole to continental areas, but also address more advanced issues such as the enlargement of pure latitudinal-longitudinal portion of the grid, the overall smooth scaling factors, and the new perspectives arisen from high-resolution and multi-scale modeling. The generated grids could potentially achieve the alignment of grid lines to coastlines, enhanced spatial resolution in coastal regions, and easier computational load balance. Since the grids are orthogonal curvilinear, they can be readily utilized by the majority of OGCMs which are based on finite difference and require grid orthogonality. These algorithms can also be applied to the grid generation for regional ocean modeling where complex land–sea distribution is present.

1 Introduction

The generation of the model grid preludes the simulation with general ocean circulation models (OGCMs) and sea ice models. Among state of the art OGCMs, including those participating in Coupled Model Intercomparison Project, the fifth phase (CMIP5 CMI, 2014) and high-resolution ocean modeling such as global oceanic forecast (e.g., Metzger et al., 2014; Storkey et al., 2010), the majority of them use orthogonal curvilinear grid (dipolar or tripolar), with the North Pole relocated to continental areas. These grids are logically Cartesian (similar to latitude-longitude grids), and usually generated by an analytical formulation, such as a Moebius Transformation, or orthogonal curves, as in Murray (1996); Murray and Reason (2001). The only land–sea distribution information that is exploited in these grids is to which continental area(s) the North Pole is to be relocated.

Contrary to OGCMs, regional ocean models (Shchepetkin and McWilliams, 2005) usually utilize orthogonal curvilinear grids that enclose the region of interest, with alignment of grid lines to coastlines. This choice is both intuitive and a well-established practice, covering the range of the study of small-scale phenomena such as river plumes (Gan et al., 2009), to basin scale modeling such as Xu and Oey (2011). The motivations behind this choice are both higher computational efficiency and better simulation: (1) it is beneficiary to align grid lines with coastlines and/or isobaths, for better simulation of the river discharge and more realistic topographic forcing on the oceanic flow; and (2) the removal of land in the grid's domain results in lower computational overhead, since lands no longer occupy the logically rectangular index space of the grid. Grid generation tools, such as SeaGrid (Sea, 2014), utilize the numerical solution of Laplacian equations and conformal mappings to ensure the orthogonality of the resulting grid. With SeaGrid, modelers need to manually specify the key vertices of the modeling region so that an orthogonal, logically rectangular grid is generated.

As an important trend for global ocean modeling, high-resolution simulation is becoming more popular for both ocean forecast (Metzger et al., 2014) and climate studies (Dennis et al., 2012). Up to 0.1° or higher nominal resolution has been successfully utilized by global models using large-scale parallel computers. With the high resolution, small scale phenomena can be resolved explicitly, such as narrow yet important water channels and mesoscale eddies, but the simulation is usually very computationally costly. To alleviate this problem, ocean modelers adopt: (1) load balancing strategies to improve computational efficiency, and (2) multi-scale modeling with spatial refinements. The load balancing algorithms exploit the fact that many grid points are inactive during the simulation as a result of the land–sea distribution (Kerbyson and Jones, 2005). On the other hand, multi-scale simulation could exploit either the spatial and temporal multi-scale characteristics of the ocean's dynamics, or the practical requirements of the spatial resolution (Mandli and Dawson, 2014; Ringler et al., 2013; Chelton et al., 1998).

In this paper, we propose two new grid generation algorithms with improvements in various aspects. They are based on advanced conformal mappings, e.g., Schwarz–Christoffel

conformal mappings. The first algorithm improves dipolar grids, with enlarged latitudinal-longitudinal (lat-lon) portion of the grid and smooth grid size and scaling factor transition. The second algorithm aims at improving existing OGCM grids in terms of better support for high-resolution and multi-scale modeling, to: (1) achieve the removal of major continents from the grid, (2) enhance spatial resolution in coastal regions, and (3) align grid lines to coastlines. Before introducing details of these algorithms, in the following part of this section, we first review the design of orthogonal curvilinear OGCM grids in Sect. 1.1, and then give a short introduction to Schwarz–Christoffel conformal mappings in Sect. 1.2.

1.1 Grids for ocean general circulation models

Ocean modeling involves: (1) the selection of an equation set, to simulate the thermodynamic and dynamic evolution of the ocean, (2) numerical treatments including spatial discretization, numerical approximation and time-domain integration. A majority of OGCMs utilize finite difference in spatial and temporal domain, and assume local orthogonality of the underlying grid. The traditional latitude-longitude grid, as a special case for general orthogonal curvilinear grids, features the convergence of meridians at the North Pole. This brings several challenges to the ocean modeling: (1) the small cell edge sizes in the zonal direction near the North Pole pose strict limitation on the time step sizes and computational efficiency, especially under the context of high resolution modeling; (2) there exists large cell size anisotropy near the North Pole, which negatively affects the effective spatial resolution. To overcome these shortcomings, current OGCMs usually utilize mappings which preserve the orthogonality and relocate the grid's pole from the North Pole, to one or several continental locations (i.e., away from the ocean).

Figure 1 shows two examples (GX1, a dipolar grid, and TX0.1, a tripolar grid) for the POP ocean model (POP, 2014) in CESM (CES, 2014). As shown, the North Pole is relocated to lands (on Greenland for the dipolar grid, and on Eurasia and North America for the tripolar grid). Also, a large portion of the grid is still lat-lon, including the low latitudes and the southern hemisphere. The benefit of the grid (or the large part of it) being lat-lon are threefold. Firstly, on the large scale, the latitudinal and longitudinal directions are characteristic for

the geophysical fluid dynamics, and the grid lines being zonal/meridional could potentially improve the simulation accuracy. Secondly, it allows easy analysis of the model output. Thirdly, the grid variables (such as latitudes and longitudes, Coriolis parameter, cell edge sizes) could be stored by one dimensional arrays, instead of the two-dimensional arrays in the general case. By reducing the memory footprint during the simulation, the model's computational performance could be improved. In fact, each of GX1 or TX0.1 consists of two patches that complement each other: (1) the southern patch that is lat-lon (i.e., the area with a latitude lower than a certain "turning latitude" ϕ); (2) the northern patch (i.e., area northern to ϕ), which contains a relocated North Pole and is not lat-lon. A non-trivial grid construction process is required to relocate the pole, during which an analytical formulation is usually adopted (as in Murray (1996)). Since there is a boundary between the northern and the southern patch, abrupt changes of grid cell edge sizes should be avoided (Roberts et al., 2006). The (local) scaling factor s (defined as the proportion of adjacent cell edge sizes) in the meridional direction should be close to 1 to ensure smooth transition.

To summarize, we outline the requirements for OGCM grids as follows. They are loosely sorted according to relative importance, starting from more important or classic ones to less important or more modern ones.

1. Grid orthogonality.
2. Relocation of grid poles to land. The further the grid poles from the ocean, the better.
3. The scaling factor is close to 1 for the whole grid, i.e., there is no jump of local grid sizes.
4. The major part of the grid is still lat-lon, for the sake of the simulation accuracy of large scale modeling especially when the spatial resolution is low, easy spatial refinement in the low-latitude oceanic regions, easy analysis of model outputs, and potential computational performance enhancements.
5. Grid size anisotropy should be low.

6. The grid does not induce very small time steps.

7. The grid is indexable as a Cartesian grid.

8. The grid can reduce unused grid points (i.e., grid points on lands) as many as possible.

9. The grid can support high resolution and multi-scale modeling.

This list is arguably more comprehensive than that in Roberts et al. (2006), with the first four items coincide with the whole list in Roberts et al. (2006) and added items to reflect new trends in ocean modeling. Item 6 through 8 are related to computational aspects. In the temporal domain, the maximum allowed time step size is crucial to the model's computational efficiency, which is constrained by the CFL condition. Hence, the grid generation method should not introduce cell edges that are too small, as is a shortcoming of pure lat-lon grids. To utilize parallel computers, OGCMs usually adopt two-dimensional domain decomposition in the horizontal spatial domain. A logically Cartesian grid is both intuitive and easy to implement, for both domain decomposition and communication management (item 7). We denote the logical indexation of the model grid as the grid index space. For item 8, since grid cells dedicated to land are not active in terms of computation and communication during the simulation, reducing their total number or proportion in the grid index space could improve efficiency and potentially exempts the need for load balancing. Item 9 is related to the aforementioned trends of high-resolution and multi-scale simulation with OGCMs. It is beneficiary that the grid could achieve higher spatial resolution where it needed (such as coastal regions, comparatively shallower regions and polar regions for resolving mesoscale eddies) and alignment of coastlines to grid lines (as in regional ocean models).

It is worth noting that Finite-Elements methods based OGCMs utilize irregular meshes (Chen et al., 2006; Wang et al., 2014; Pain et al., 2005, e.g.,), and could potentially achieve multi-scale ocean modeling. But it is impossible for the majority of existing OGCMs to adopt irregular meshes, which requires re-formulation of the numerical treatments of the equations from scratch. In this paper, one of the proposed algorithms targets at providing a basis for the multi-scale modeling with the large body of existing OGCMs, by using Schwarz–

Christoffel mappings to achieve land removal and enhanced spatial resolution in coastal regions.

1.2 Schwarz–Christoffel conformal mapping

Conformal mappings (Nehari, 1975) are angle-preserving transformation on the complex plane. As a most simple conformal mapping, the Moebius transformation has been used to generate dipolar grids for OGCMs (Murray, 1996). A Moebius transformation $z = \frac{a*z+b}{c*z+d}$ is constructed to: (1) map the northern patch (under stereographic projection) to the unit disk, and (2) map the grid's north pole (a user-specified position, e.g., on Greenland) to origin of the unit disk. Once the conformal mapping is constructed (i.e., the variables a, b, c and d are computed), a polar coordinate could be constructed on the unit disk and mapped back to form the grid on the northern patch. Since: (1) the Moebius transformation is angle-preserving, (2) the polar coordinate is orthogonal, and (3) forward and backward stereographic projections preserve angles, it is guaranteed the grid for the northern patch is orthogonal. Figure 2 shows the grid constructed by a Moebius transformation for the northern patch of a turning latitude of 20° N and the conformal center on Greenland (45° N, 40° W). Note that the maximum and minimum of scaling factors of the grid is $d2/d3$ and $d1/d3$, which are 1.66 and 0.66 respectively, which are far from 1.

For a single-connected region R with an irregular boundary (e.g., not a circle for a uniform turning latitude), instead of a Moebius transformation, a Schwarz–Christoffel (SC) conformal mapping (Driscoll and Trefethen, 2002) is needed for the mapping between a unit circle and R. For a polygon boundary with n vertices: $\{v_i | 1 \leq i \leq n\}$ and internal angles of $\{\phi_i | 1 \leq i \leq n\}$, the SC mapping f from the unit disk to the region enclosed by the polygon could be defined as:

$$f(z) = A + C \int^{z} \prod_{i=1}^{n} (1 - \frac{\zeta}{z_i})^{\left(\frac{\phi_i}{\pi}\right)} d\zeta \tag{1}$$

Where A and C are scalar constants, and z_i's correspond to v_i's under the SC mapping. The values of A, C and z_i's could be numerically computed through a construction process (Driscoll and Trefethen, 2002). Figure 3 shows an example in which an SC mapping is generated for a user-defined polygonal area, generated with SCToolBox (SCT, 2012). Vertices v_i's of the polygon and corresponding vertices on the unit circle (z_i's) are shown. The polar coordinate on the unit disk is constructed and mapped with f to form an orthogonal grid on the polygonal region (potentially a northern patch).

For a multiple-connected region with a connectivity of n ($2 < n < \infty$), e.g., a complex plane with $n-1$ non-intersecting areas, there exist canonical forms that this region could be mapped to (Chapter 7 of Nehari (1975)). Figure 4 shows a sample region with connectivity of 5, and its canonical forms under Schwarz–Christoffel mappings. For a complex plane with polygonal regions as in Fig. 4.a, an SC mapping exists that map this plane to another plane, on which the polygons are mapped to: (1) circles, as in Fig. 4.b, (2) parallel line segments, as in Fig. 4.c, (3) radial line segments, as in Fig. 4.d, or (4) circular line segments in Fig. 4.d. Note that the conformal invariant point, i.e., the point whose position remains unchanged, is marked out by a steroid on each complex plane.

Despite that the canonical forms of multiple-connected regions have long been recognized, how to construct a Schwarz–Christoffel mapping between a user-specified polygonal area and a canonical form is a recent discovery since Delillo et al. (2004). In this paper, we omit the technical details for SC mapping construction as introduced in DeLillo and Kropf (2011); DeLillo et al. (2013), and focus on their application in grid generation for OGCMs.

Hereby we denote SCSC as the Schwarz–Christoffel mapping for single-connected region, and MCSC the Schwarz–Christoffel Mapping for multiple-connected regions. In Sect. 2, we apply SCSC to improve existing dipolar grids. In specific, we improve the patching scheme, by designing a North Polar cap with an irregular boundary instead of a uniform turning latitude, to enlarge the lat-lon portion of the dipolar grid. By using SCToolBox for implementation, we construct an SCSC mapping to generate the orthogonal grid for the North Polar cap. In Sect. 3, we treat the continental part of the earth as a set of enclosed regions (with irregular boundaries), denoted as C, and remove C by constructing an MSCS map-

ping to map C to a set of slits. Hence a grid can be constructed with continents removed and grid lines aligned to continental boundaries. The open-source software of MCSC (MCS, 2013) is used for the construction the conformal mapping. For each grid generation algorithm, we provide a sample grid for: (1) the static evaluation, and (2) idealized simulation with POP, to validate that they can be easily adopted by OGCMs. Then in Sect. 4, extensions to the proposed methods and the relationship with existing ones are discussed. Finally, Sect. 5 concludes the article.

2 Pole Relocation with SCSC Mappings

In this section we apply the Schwarz–Christoffel mapping for single-connected region (SCSC) to the generation of dipolar grids for OGCMs. We mainly address the following grid design topics: (1) the enlargement of the portion of the regular latitudinal-longitudinal part; (2) the mitigation of scale changes across patch boundaries; (3) reduced grid size anisotropy in polar regions. Traditional dipolar grids (Murray, 1996; Roberts et al., 2006) usually contain: (1) a northern patch and a southern patch, divided by a turning latitude, (2) regular lat-lon grid for the southern patch, and (3) an analytical form based, non lat-lon grid in the northern patch. To reduce the non lat-lon portion of the grid (50 % for GX1 and 28 % for TX0.1 as shown in Table 1), we design a new patching scheme, which can shrink the portion to as low as 6 %, while maintaining the overall smooth transition of scaling factors.

The patching scheme is shown in Fig. 5, in which the earth's surface is divided into 5 patches. Central to the grid generation algorithm is a northern patch with an irregular, non-longitudinal southern boundary. We denote it the North Polar cap patch (NP). It includes a relocated pole on Greenland, and a smooth but irregular, non-longitudinal boundary with 4 segments, as listed below.

- Longitudinal segment across the Atlantic Ocean at a certain latitude (at 47 N), which extends into Eurasia and North America on both ends;

- Longitudinal segment across the Pacific Ocean at a certain latitude (across Bering Strait), which extends into Eurasia and North America on both ends;
- Linkage for the first two segments on Eurasia;
- Linkage for the first two segments on North America.

The last two segments, which are on the continents, are constructed to ensure that the overall boundary is smooth. Due to the irregular boundary of NP, an SCSC mapping is constructed to map: (1) a unit disk to the stereographic projection of NP; (2) the origin of the unit disk to the prescribed continental position on Greenland (i.e., the location for the grid's pole).

Patches southern to NP are: (1) the southern patch (SP), to cover the mid and high latitudes in the southern hemisphere; (2) the equatorial band patch (EBP), to cover low latitude areas (with meridional refinement); (3) the north Pacific patch (NPP), covering the area between EBP and NP on the Pacific Ocean and Indian Ocean; and (4) the north Atlantic patch (NAP), covering the leftover area between EBP and NP (which mainly corresponds to the North Atlantic ocean). The boundaries between NPP and NAP are meridional and on continental masses, i.e., Eurasia and North America.

Furthermore, we construct the oceanic part of NPP and NAP to be lat-lon (and orthogonal). The leftover, non-oceanic areas in NPP and NAP are filled with non-orthogonal grid cells. Since the grid points in these areas are not active in the simulation, it is guaranteed that the loss of orthogonality of these points does not affect simulation results. During the construction of each patch, meridional refinements are introduced where the grid size anisotropy is large.

The grid generation algorithm is outlined as follows:

1. Generation of the NP boundary.
2. Grid generation for NP, by constructing an SCSC mapping from a unit-disk to the stereographic projection of NP. An orthogonal, a polar coordinate is generated for

the unit disk, and mapped back by the SCSC mapping and backward stereographic projection. The meridional grid cell sizes along the NP boundary are computed.

3. Generation of the Pacific and North Atlantic basin patches, i.e., NAP and NPP. Linkage between: (1) NAP and NPP on eastern and western boundaries, (2) NAP (or NPP) and NP are also constructed.

4. Generation of the equatorial and southern grid patches, i.e., EBP and SP, according to grid cell anisotropy requirements.

5. Assembly of the patches into a global grid.

6. Generation of land and depth masks.

As a consequence of the choice of the boundary and conformal center of NP, the cell sizes along its boundary are not uniform. Because Atlantic Ocean and Pacific Ocean are not directly connected between 40° N and 70° N, different meridional grid edge sizes in these two basins could be used to mitigate the difference in the meridional step sizes between the NP-NPP boundary and NP-NAP boundary.

Before introducing the detailed design, we show a sample grid with nominal 1 ° resolution (360×306) in Fig. 7, with detailed view of the North Polar region. One in every five grid points are shown in both directions. A large portion of the Pacific and Atlantic Ocean are lat-lon. The patch boundary between NPP and NAP are not smooth, since the orthogonality in these continental regions is not ensured.

2.1 Settings for the NP

The choice for the boundary of NP is the trade-off among several factors: the reduction of the length of the boundary on the Pacific and Atlantic Ocean, the smoothness of the scaling factor in both meridional and zonal directions, etc. In the sample grid, we choose: (1) on the Pacific side, the longitudinal segment crossing Bering Strait, i.e, at about 66° N, from 170° N to 160° W; (2) on the Atlantic side, the longitudinal segment at about 48° N, from

70° N to 0° N; (3) the smooth linkage between the two segments on North American and Eurasian continent respectively; (4) the relocation of the grid's pole to Greenland (78° N, 42° N). The smoothness is ensured by constructing a cosine function shaped curve in the latitude-longitude space. Suppose we need to link a point at (lat_1, lon_1) and another point at (lat_2, lon_2), with smooth linkage to longitudinal lines on both ends. The latitude lat on a specific point on the link at certain longitude lon could be written as a function of the longitude:

$$lat = lat_1 + (lat_2 - lat_1)\frac{1 - cos(\frac{lon - lon_1}{lon_2 - lon_1} \times \pi)}{2} \tag{2}$$

The scheme is shown in Fig. 6.a. Approaching both ends of the link, i.e., (lat_1, lon_1) and (lat_2, lon_2), the line is gradually parallel to and joined with the specific longitudinal lines. Hence the overall smoothness is achieved.

We use a discretized boundary (nominal resolution in the zonal direction) as the polygon boundary to construct the SCSC mapping. The NP boundary is shown in Fig. 5 in blue lines. The grid lines are both orthogonal internally within NP and perpetual to the boundary of NP.

2.2 Control of grid anisotropy

For dipolar grids, grid cells in the polar regions tend to feature very large anisotropy in cell sizes. Meanwhile, equatorial regions are often modeled with higher meridional resolution for purposes such as higher accuracy in the simulation of tropical waves and ENSO (Griffies et al., 2000). One example is GX1 (shown in Fig. 1.a), in which the grid cell anisotropy (meridional edge size divided by zonal edge size) in the tropics is about 4.24.

In the proposed grid generation method, we introduce a bespoken threshold value to limit the maximum anisotropy in polar regions. This value is also used for the meridional refinement in EBP. Hence the maximum grid size anisotropy of the whole grid is kept below this value. For SP, due to that it is purely lat-lon, the latitudes and longitudes of the grid points

could be computed as one dimensional arrays. We start from the lowest latitude (southern boundary of EBP) and numerically integrate to higher latitudes by gradually decreasing the sizes of latitudinal steps. The speed for meridional step size shrinkage are designed to ensure that the maximum anisotropy does not increase beyond the predefined threshold. For NP, a similar strategy to gradually reduce the latitudinal steps is used, except that due to the uneven edge sizes for any zonal circle, the anisotropy of a certain zonal circle of the grid is computed as the average meridional edge size divided by the average zonal edge size on the circle.

One important property of the anisotropy control scheme is that although it increases the number of unknowns, it does not induce reduction of maximum time step size during the simulation. The maximum time step size is the global minimum of the the local maximum time step sizes, denoted $t_{max}^{(i,j)}$ at index (i, j) , as constrained by the local CFL conditions. With either explicit or semi-implicit numerical integration, $t_{max}^{(i,j)}$ is proportional to the smaller one of the meridional and the zonal cell edge sizes. In the polar region, it is usually the zonal edge that constrains $t_{max}^{(i,j)}$. The control of anisotropy introduces more meridional steps, but has no effect on the zonal edge size. Therefore, it does not further decrease the maximum time step size that is allowed for the simulation.

2.3 Mitigation of scaling factors

As introduced above, to maintain the accuracy of finite difference operators, the local scaling factors should be close to 1. To ensure that there is abrupt scale changes across the boundary of NP, after the grid generation for NP, we compute the the cell edge sizes along the two oceanic segments of NP boundary as the average meridional cell edge size of all the cells on each of the segments. Then, NAP and NPP are treated separately to ensure a smooth transition of meridional edge sizes, starting from the uniform meridional edge size in the south (i.e., the boundary with EBP), and gradually changing to to the meridional edge sizes on its northern boundary with NP. We use a cosine function to construct the meridional edge sizes: (1) on both southern and northern ends the transition of cell sizes is

smooth, and (2) the numerical integration (i.e., the sum) of all the meridional edges equals the latitude difference between EBP and NP. This scheme is shown in Fig. 6.b. The count of meridional points for NAP and NPP should be the same, to ensure that the grid is still addressable as a Cartesian grid. Therefore, there exists difference in the meridional edge sizes in NAP and NPP.

Within EBP, since the meridional refinement is adopted, a similar scheme for smooth transition is also used, as shown by the example grid in Fig. 7.

The meridional and zonal grid edge size of the sample grid is shown in Fig. 8.a and b in grid index space, and the anisotropy (meridional edge size divided by zonal edge size) shown in Fig. 8.c. The value of the anisotropy threshold for constructing the sample grid is 3. As is shown, the overall anisotropy is kept under 3. As a result, more grid points are dedicated to the Arctic Ocean, with enhanced resolution to resolve the important passages such as Nares Strait and Lancaster Sound. The effect of scaling factor mitigation is shown in Fig. 8.d (with areas of the scaling factor larger than 1.1 marked out by black contours). The north Atlantic Ocean part is shown, where the boundary between NAP and NP and the largest scaling factor of the global grid is present. As is shown, the scaling factor is kept lower than 1.1 for most part of the area, and only exceeds 1.1 by the eastern end of the patch boundary.

In the sample grid, the lat-lon part covers 93.8 % of the total oceanic area. Compared with traditional dipolar grids (as in Roberts et al. (2006)), in which about 75.3 %, 79.0 % and 82.2 % of the earth's oceanic part is covered by regular latitude-longitude part for the turning angles of 20° N, 25° N and 30° N respectively, the proposed dipolar grid achieves a much higher lat-lon occupation. Actually this proportion is similar to that achieved by a tripolar grid (96 %) with High Latitude Transition (HLT, as in Murray (1996)) with a polar patch starting at 66° N. It is worth noting that however the high lat-lon portion of the HLT grid, the undesired large scaling factor is present. The advantages over existing dipolar grids are achieved through: (1) the irregular boundary which allows more of the oceanic part to be included by lat-lon portion of the grid, and (2) non-orthogonal grid cells with abrupt scale changes that

reside on the continents and do not affect simulation. The proposed grid generation method exploits more land–sea distribution information for the grid construction.

2.4 Evaluation with OGCM simulation

Since the sample grid is an orthogonal curvilinear grid, it can be utilized by the majority of OGCMs. We evaluate the sample grid from the following aspects: (1) the static evaluation in terms of the maximum allowed time steps and comparison with existing dipolar grids, and (2) the application of the grid in POP.

With the assumption of an (split) explicit formulation, we show the global map of the minimum count of time steps per simulation hour for the external gravity wave (i.e., the barotropic mode) in Fig. 10.a. The local minimum time step count is defined as: $\frac{3600s}{min(\Delta_x,\Delta_y)/\sqrt{gh}}$, where Δ_x and Δ_y are the local cell edge sizes in the grid's meridional and zonal direction respectively, g the gravity acceleration, and h the ocean depth at the cell.

Similar to traditional dipolar grids (e.g., GX1), the critical area with respect to barotropic time step size is in the Arctic, near the Greenland, as the result of: (1) small zonal edge sizes, and (2) the large external gravity wave speed. The sample grid is comparable to GX1 in terms of the minimum allowed time step count per simulation hour (86.0 versus 57.6 for GX1 which has lower zonal resolution of 1.125° and a shallower Arctic basin).

We further implemented the grid in POP. We generate the grid's depth mask field by interpolation and discretization on 46 depth levels. The depth for each vertical layer starts from 3 meters for the surface layer, to 250 meters in the deep ocean. The global maximum depth is 6000 meters. Simulation with idealized forcing is carried out to demonstrate that the sample grid can be easily utilized by OGCMs. The configuration of the simulation is as follows: (1) the potential temperature and salinity is initiated to a vertical climatological profile (POP, 2014); (2) the model is forced by analytical, latitude-based wind stress and surface heat forcing (with SST restoring) that is constant in time, shown in Fig. 9.a and b, respectively ; (3) the spin-up is 10 years. In Fig. 10.b and c, we show the mean surface temperature field (SST) of the first month after the spin-up, and a snapshot of the magnitude of the surface flow field, respectively. It is shown that under the analytical forcings, the

model could reproduce reasonable SST distribution and large-scale oceanic flow such as equatorial and western-boundary currents. This provides validation that the grid could be integrated as a swap-in option in existing OGCMs. The further application of the grid in ocean modeling and climate studies serves as future work, including: (1) refined boundary information for the grid construction, (2) the long-term spin-up with realistic forcings, and (3) simulation with coupled models.

3 Grid generation with MCSC mappings

In this section we propose the second grid generation method for OGCMs. It targets at the new trends of high-resolution and multi-scale ocean modeling (item 8 and 9 in the list in Sect. 1). By utilizing Schwarz–Christoffel conformal mappings for multiple-connected regions (MCSC), we remove major continental masses from the grid, by mapping them to slits with no area. Similar to the sample grid in Sect. 2, the resulting grid is orthogonal curvilinear, and can be utilized by the majority of OGCMs. It can potentially achieve: (1) the removal of major continental masses from the grid index space, (2) higher spatial resolution in coastal regions, and (3) the alignment of the large-scale coastlines to the grid lines.

The outline of the grid generation method is as follows.

1. Manual selection of the polygonal boundary for each continental mass that are to be mapped to slits. The area enclosed by the polygon should be strictly inland.

2. Construction of an MCSC mapping f between the two following complex plane: (a) the complex plane p_e, which is the stereographic projection of the earth, and (b) a complex plane p_s on which the aforementioned polygonal continental areas are mapped to slit regions.

3. According to the grid resolution requirement, a polar grid coordinate system is generated on p_s and mapped back to p_e with f, and further onto the globe through backward stereographic projection to form the model grid.

4. Generation of land and depth masks.

The mapping scheme between p_e and p_s is shown in Fig. 11.a.

Because of: (1) the orthogonality of the polar coordinates on p_s, (2) the angle-preserving property of f, and (3) the properties of the stereographic projection, the orthogonality of the grid is guaranteed. The resulting grid features several unique properties. On p_s, the grid points close to the slits are mapped to physical positions close to continental boundaries on p_e. On p_s, the circular slits are parallel to circular grid lines of the polar coordinate, and the radial slits to radial grid lines. The parallelism between grid lines and slits are translated onto p_e by f. The closer the grid points are to a slit on p_s, the better alignment of grid lines (in either direction) to the corresponding continental boundary is, which a result of harmonics behavior of the conformal mapping. Since slits have zero area on p_s, the grid lines that cross any slit on p_s will be long, curved lines on p_e. Because only the inner boundaries of the continental masses are chosen to be mapped to slits, the grid lines crossing slits and their corresponding grid cells only reside on lands, and are inactive during the simulation of the ocean. Hence the removal of major continental mass in the grid index space (i.e, I–J space) is achieved. Note that as the lateral boundary of the oceans (hence lateral boundary condition for the model), the coastlines are still present in the grid.

For the numerical implementation, we use an adapted version of the open-source software MCSC (MCS, 2013) for the generation of f, with code changes and augmentations to accommodate the mixed type of slit maps (i.e., radial and circular slits at the same time). We evaluate the grid generation method through a sample grid, which is generated with a basic, manually chosen set of the continental areas. In the following part of this section, we cover the details of the grid design, the basic evaluation of the sample grid, and verification with OGCM simulation.

3.1 Continental boundary and slit choices

For the sample grid, we limit the choice of the polygonal boundaries for continents to those enclosed by manually picked points. The number of points per continent (i.e., the vertices

for corresponding polygons) is kept small, so that it is feasible to choose by hand. It is also ensured that the region enclosed by the polygon is strictly inland, to guarantee that no oceanic region is mapped to slits. The scheme presented here is basic, and only used to demonstrate the grid generation methodology. More advanced schemes, such as: (1) a spline based smooth boundary generated from manually picked in-land points, or (2) automatically retrieved continental boundaries, are also possible but beyond the scope of this paper.

Each polygonal area, representing a continent, is mapped to a slit in p_s. It can be mapped to either a circular or a radial slit, as introduced in Sect. 1. The slit type of each area can be specified by the user by subjective judgments based on the shape of the area. For example, in Fig. 11, Eurasia, Africa, North America and South America are mapped to a set of two circular slits (for Eurasia and North America) and two radial slits (for Africa and South America).

We construct the sample grid with the 4 major continental masses, as listed in Table 2. The conformal center for p_s and p_c is on Greenland (77.5° N, 41° N), which serves as the geographic location of the grid's north pole. The corresponding polygonal areas are shown as blue or red colored patches in Fig. 12.a, with blue ones mapped to circular slits and red ones to radial slits on p_s. For the Eurasia continent, Black Sea and Caspian Sea are omitted as oceanic regions, hence they are included in the polygonal area of the Eurasia continent. For North America, Greenland is omitted since it contains the conformal center. Africa is divided into two parts as the result of its special shape: the northern part mapped to a circular slit and the southern part mapped to a radial slit. Along the south-east coastline of China, several extra points are added, to demonstrate that the grid lines can be forced to follow coastlines more closely if needed.

3.2 Basic evaluation of sample grid

We focus on two aspects for the basic evaluation of the sample grid: (1) the effect of the continental area removal, and (2) the alignment of grid lines to coastlines. As shown in Table 2, the proportion of areas that are mapped to slits on the continents are close to or

over 60 %. It is worth noting that this is the result of the specific choice of polygons for the sample grid. If a high-resolution grid is to be constructed, the choice of in-land points could be refined to more closely fit coastlines. For the sample grid, the in-land points are chosen to be at least 100 km from any seas. On the earth, these areas (at least 100 km away from any seas) accounts for 80 % of the total land area. Hence the removed area is over 80 % of the total removable area, with respect to the 100 km threshold. Besides, we don't consider peninsula and archipelagos, which also lowers the proportion of the area removal.

Figure 12 shows the global sample grid and details in specific regions. The sample grid is nominal 0.25° in resolution, and one in every 10, 10, 2, 2 and 4 points are plotted in the sub-figures, respectively. As shown in Fig. 12.b, the grid lines in the North-Polar region are well constrained by the two major continental boundaries, in particular Hudson Bay. Since regions such as the Scandinavian Peninsula, Canadian Arctic Archipelago, Indochina and Iberian Peninsula are not included, grid lines are not forced to align with coastlines in these regions. But it is worth to note that: (1) the land–sea distribution in these regions are still present in the grid, providing the necessary lateral boundary condition for the OGCM, and (2) the resolution in these regions, especially among archipelagos are enhanced, since the grid points that were dedicated to lands are now redistributed and to resolve these regions better. The alignment of grid lines to coastlines is a collateral result of the alignment of grid lines to the polygon boundaries. Since the hand-picked polygon boundary only reflect the large-scale land–sea distribution information, the alignment of grid lines to actual coastlines is only at the largest scale. Figure 12.c and d show that coastlines are closely aligned to grid lines where more points are used for detailed control of the polygon boarders.

The actual land–sea distribution and grid cell edge sizes in the grid index space are shown in Fig. 13. The slits on p_s correspond to one dimensional arrays (constant-I or constant-J) in the grid index space. They are marked in corresponding colors as in Fig. 12. It is shown that major continental masses are removed from the grid index space. Although Figure 13 is not directly recognizable as global maps, it is still immediate to which part the oceans correspond to. There are some large cell sizes present on the oceanic areas, es-

pecially at the slit tips of each corresponding boundary. This could be improved through modifications to the positions of hand-picked in-land points.

Through the static evaluation of the grid, we show that the sample grid satisfies the three major aforementioned features: (1) the removal of major continental masses from the grid index space, (2) the alignment of coastlines to grid lines, and (3) enhanced spatial resolution at coastal areas. It is worth to note that these three features are achieved at the same time, as a result of the conformal mapping and its harmonics behavior. Besides, if desired, the effect of grid line alignment and continental removal could be improved through a better, more detailed boundary information that is used for constructing the MCSC mapping.

3.3 Evaluation with OGCM simulation

We evaluate the sample grid under the same protocol as in Sect. 2, i.e., in terms of the minimum time step count per simulation hour, and the simulation result with POP under idealized forcings. The sample grid used for simulation is nominal 0.5° (720 by 330), and the simulation was carried out following the same protocol for model initialization, settings for forcings, etc.

In Fig. 14.a, it is shown that the most critical area in restricting the time step sizes is also the Arctic region close to Greenland, with respect to the external gravity wave speed and an (split) explicit model formulation. The minimum time step count per simulation hour is 113.7. As compared with the sample grid generated with SCSC mapping (1° nominal zonal resolution with 86.0 steps per hour) and GX1 (1.125° nominal zonal resolution with the global maximum depth of 5500 meters and 57.6 steps per hour), the sample grid is comparable in terms of the maximum allowed time step size.

Figure 14.b and c show the mean SST field and a snapshot of the surface flow field after the model spin-up. Similar to the sample grid in Sect. 2, the sample grid generated with MCSC mapping yields reasonable SST distribution and surface flow field. This justifies that the grid could be integrated with existing OGCMs as a swap-in option. The further application of the associated grid generation method include refined continental boundaries that

are used for the generation of the MCSC mappings, and long-term ocean ocean simulations with realistic atmospheric forcings.

4 Related Work & Discussion

In this article, advanced conformal mapping techniques, namely, Schwarz–Christoffel mappings are used to generate orthogonal grids for ocean general circulation models. These orthogonal, curvilinear grids are indexable in a regular Cartesian manner, and can be easily integrated with existing OGCMs which already supports orthogonal curvilinear grids, such as POP or NEMO (NEM, 2014).

Spatial discretization with irregular and non-orthogonal grids are used by algorithms such as finite-elements or finite-volume methods, which are widely used in the fields such as computational fluid dynamics and structure design. In recent years, these non-structured grids are also being adopted in ocean modeling, such as FVCOM (Chen et al., 2006), MPAS-Ocean (Ringler et al., 2013), FESOM (Wang et al., 2014), ICOM (Pain et al., 2005), etc. Despite certain limitations as listed in Griffies et al. (2010), these models have shown advantages under the context of multi-scale modeling (Chen et al., 2009; Scholz et al., 2013, e.g.). On the contrary, traditional OGCMs based on structured meshes usually provide multi-scale simulation capabilities through nested grids with one-way forcing or two-way coupling. The proposed grid generation method in Sect. 3 levitates traditional OGCMs, providing them a basis for multi-scale simulation. Grid points that were dedicated to lands are redistributed to oceanic areas, with coastal area with potentially higher density of grid points. By combining with other dynamic or static spatial refinement strategies, an overall multi-scale ocean simulation could be carried out, such as adaptive grid resolution with respect to the spatial scale distribution of mesoscale eddies.

The sample grid in Sect. 3 does not have latitude-longitude grid along the equator. It is worth to note that this is is not due to the limitation of the methodology. For example, extra polygons on p_e could be added for the equatorial lines on both the Atlantic and Pacific Ocean (which correspond to circular slits on p_e), and the conformal map could be con-

structed to map these polygons to two circular slits on p_s. Hence the alignment of grid lines to the equator is achieved.

In Murray (1996), a grid generation method was proposed to utilize the conformal equivalence of the orthogonal grid with an electrostatic field. This approach, denoted Multi-Polar algorithm (MP) is able to remove some land area from the grid, by placing two points with positive and negative charges on the same continent (e.g., Eurasia, Antarctica). Although different in motivation, this approach and the one proposed in Sect. 3 bear certain similarity in the capability to remove continental areas. However in MP, the modeler does not have direct control of the area to be removed. For effective removal of continental mass, extra efforts are needed, including: (1) a variable number of charged points, with variable values of charge, and (2) the numerical optimization of these values to approximate the real continental boundaries. Instead, with the proposed method based on MSCS mapping, modelers have direct control over the area to be removed, by specifying the polygonal areas and the specific slit type for each area.

The invariance of the solution of a Laplacian equation with 1st or 2nd type boundary condition under conformal mappings could be further utilized for grid generation. Instead of the construction of the conformal mapping, a numerical solution of boundary value problem is needed. The 1st and 2nd type boundary conditions are equivalent to the circular and radial slits as in the approach in Sect. 3, assuming that the grid's pole on Greenland and the South Pole have the 1st type boundary condition.

The MCSC mapping based grid generation method could also be applied to the generation of grids for regional ocean models such as ROMS (Shchepetkin and McWilliams, 2005), especially for regions with complex land–sea distribution such as Canadian Arctic Archipelago or South East Asia. For traditional grid generation methods, the multiple connectivity of land areas in these regions poses a special challenge, as well as narrow but hydrologically important water channels. The proposed algorithm in Sect. 3 potentially serves as a framework to overcome both problems.

In the supplements, we provide the grid input file for POP in binary format for the two sample grids, with nominal 1° and 0.5° resolution, respectively. Integration with other OGCMs

require the conversion of grid input formats and the interpolation of initial states, etc. The two grid generation methods in this paper are implemented in MATLAB, which utilize open source softwares of SCToolBox and MCSC. We plan to provide the two grid generation software in open source format, with which users could specify various grid settings such as spatial resolution, etc. The generation of the SC mappings, as compared with analytical forms based grid generation methods, is much more computationally intensive. One notable shortcoming of MATLAB is the limited performance as compared with C language or FORTRAN based implementations. Since the grid generation task is only carried out once for a whole set of simulations (the spin-up run or the coupled model simulation, etc.), currently we only focus on the functionality aspects of the methods. The optimization in terms of the computational performance is postponed to future works.

5 Conclusions

In this paper, we propose two new grid generation methods for global ocean generation circulation models. Contrary to conventional dipolar or tripolar grids based on analytical formulations, these new methods are based on Schwarz–Christoffel (SC) conformal mappings with user-defined boundary information. The first method improves the conventional dipolar grids. With SCSC mapping, it constructs an orthogonal North-Polar patch with a smooth but a irregular southern boundary. By utilizing the disconnectedness of major ocean basins in the mid-latitudes in the northern hemisphere, the local scaling factors across patch boundaries are kept low. In the sample grid, 93.8 % of the oceanic area is still covered by regular latitude-longitude grid, which is higher than conventional dipolar grids or tripolar grids.

The second grid generation method aims at more modern topics in ocean modeling: (1) the removal of major continental masses from the global grid, (2) better resolution at coastal regions with alignment of coastlines to grid lines, and (3) the support for multi-scale simulation. This is achieved by constructing an MCSC mapping, which maps the continental areas to slit regions. As a consequence, these areas correspond to one dimensional grid cells in the grid index space. Also the conformal mapping ensures the alignment of grid

lines with the boundaries of these areas, hence the approximate alignment with coastlines. Oceanic regions near these boundaries are packed more densely with grid points, which corresponds to better spatial resolution in coastal regions. Compared with conventional analytical form based grid generation methods, this method exploits more information of land–sea distribution in the form of bespoken continental boundaries.

Through static evaluation and simulation with 3-D ocean model (POP), we show that the sample grids can readily serve as replacements for existing grids in the majority of OGCMs which readily support orthogonal curvilinear grids. The MCSC based grid generation method could also be combined with other dynamic or static spatial refinement methods to achieve multi-scale ocean modeling. As the first aspect of the future work, we plan to further apply the proposed methods with more refined boundary information during grid construction and long-term numerical integration with realistic forcings for OGCM spin-up. We also plan to formulate the proposed methods into a complete, open-source grid generation software for both global and regional ocean models.

Acknowledgements. We would like to thank the editors and the referees for their invaluable effort in improving this paper. This work is partially supported by National Science Foundation of China under grant no. 41205072 and 51190101.

References

Schwarz-Christoffel Toolbox for MATLAB, http://www.math.udel.edu/~driscoll/SC/, [accessed 19-Nov-2014], 2012.

Multiply Connected Schwarz-Christoffel Mapping, https://bitbucket.org/ehkropf/mcsc, [accessed 11-Nov-2014], 2013.

CESM | Community Earth System Model, http://www.cesm.ucar.edu, [accessed 25-Nov-2014], 2014.

Coupled Model Intercomparison Project Phase 5 - Overview, http://cmip-pcmdi.llnl.gov/cmip5/, [accessed 12-Oct-2014], 2014.

NEMO – Nucleus for European Modelling of the Ocean, http://www.cmcc.it/models/nemo, [accessed 20-Nov-2014], 2014.

CESM1.1: Parallel Ocean Program (POP2), http://www.cesm.ucar.edu/models/cesm1.2/pop2/, [accessed 25-Nov-2014], 2014.

SeaGrid for Matlab, http://woodshole.er.usgs.gov/operations/modeling/seagrid/index.html, [accessed 20-Nov-2014], 2014.

Chelton, D. B., deSzoeke, R. A., Schlax, M. G., Naggar, K. E., and Siwertz, N.: Geographical variability of the first baroclinic rossby radius of deformation, J. Phys. Oceanogr., 28, 433–460, 1998.

Chen, C., Beardsley, R., and Cowles, G.: An unstructured grid, finite-volume coastal ocean model (FVCOM) system, Oceanography, 19, 78 – 89, doi:http://dx.doi.org/10.5670/oceanog.2006.92, 2006.

Chen, C., Gao, G., Qi, J., Proshutinsky, A., Beardsley, R. C., Kowalik, Z., Lin, H., and Cowles, G.: A new high-resolution unstructured grid finite volume Arctic Ocean model (AO-FVCOM): An application for tidal studies, Journal of Geophysical Research: Oceans, 114, n/a–n/a, doi:10.1029/2008JC004941, http://dx.doi.org/10.1029/2008JC004941, 2009.

DeLillo, T. and Kropf, E.: Numerical Computation of the Schwarz–Christoffel Transformation for Multiply Connected Domains, SIAM Journal on Scientific Computing, 33, 1369–1394, doi:10.1137/100816912, http://dx.doi.org/10.1137/100816912, 2011.

Delillo, T., Elcrat, A., and Pfaltzgraff, J.: Schwarz-Christoffel mapping of multiply connected domains, Journal d'Analyse Mathematique, 94, 17–47, doi:10.1007/BF02789040, http://dx.doi.org/10.1007/BF02789040, 2004.

DeLillo, T., Elcrat, A., Kropf, E., and Pfaltzgraff, J.: Efficient Calculation of Schwarz–Christoffel Transformations for Multiply Connected Domains Using Laurent Series, Computational Methods and Function Theory, 13, 307–336, doi:10.1007/s40315-013-0023-1, http://dx.doi.org/10.1007/s40315-013-0023-1, 2013.

Dennis, J. M., Vertenstein, M., Worley, P. H., Mirin, A. A., Craig, A. P., Jacob, R., and Mickelson, S.: Computational performance of ultra-high-resolution capability in the Community Earth System Model, International Journal of High Performance Computing Applications, 26, 5–16, doi:10.1177/1094342012436965, http://hpc.sagepub.com/content/26/1/5.abstract, 2012.

Driscoll, T. A. and Trefethen, L. N.: Schwarz-Christoffel Mapping, Cambridge University Press, 2002.

Gan, J., Li, L., Wang, D., and Guo, X.: Interaction of a river plume with coastal upwelling in the northeastern South China Sea, Continental Shelf Research, 29, 728 – 740, doi:http://dx.doi.org/10.1016/j.csr.2008.12.002, http://www.sciencedirect.com/science/article/pii/S0278434308003713, 2009.

Griffies, S., S, Adcroft, A., Banks, H., B¨oning, C., Chassignet, E., Danabasoglu, G., Danilov, S., Deleersnijder, E., Drange, H., England, M., Fox-Kemper, B., Gerdes, R., Gnanadesikan, A., Greatbatch, R., Hallberg, R., Hanert, E., Harrison, M., Legg, S., Little, C., Madec, G., Marsland, S., Nikurashin, M., Pirani, A., Simmons, H., Schr¨oter, J., Samuels, B., Treguier, A.-M., Toggweiler, J., Tsujino, H., Vallis, G., and White, L.: Problems and Prospects in Large-Scale Ocean Circulation Models, Proceedings of OceanObs'09: Sustained Ocean Observations and Information for Society, doi:doi:10.5270/OceanObs09.cwp.38, 2010.

Griffies, S. M., Böning, C., Bryan, F. O., Chassignet, E. P., Gerdes, R., Hasumi, H., Hirst, A., Treguier, A.-M., and Webb, D.: Developments in ocean climate modelling, Ocean Modelling, 2, 123 – 192, doi:http://dx.doi.org/10.1016/S1463-5003(00)00014-7, http://www.sciencedirect.com/science/article/pii/S1463500300000147, 2000.

Kerbyson, D. J. and Jones, P. W.: A Performance Model of the Parallel Ocean Program, International Journal of High Performance Computing Applications, 19, 261–276, doi:10.1177/1094342005056114, http://hpc.sagepub.com/content/19/3/261.abstract, 2005.

Mandli, K. T. and Dawson, C. N.: Adaptive mesh refinement for storm surge, Ocean Modelling, 75, 36 – 50, doi:http://dx.doi.org/10.1016/j.ocemod.2014.01.002, http://www.sciencedirect.com/science/article/pii/S1463500314000031, 2014.

Metzger, E., Smedstad, O., Thoppil, P., Hurlburt, H., Cummings, J., Wallcraft, A., Zamudio, L., Franklin, D., Posey, P., Phelps, M., Hogan, P., Bub, F., and DeHaan, C.: US Navy operational global ocean and Arctic ice prediction systems, Oceanography, 27, 32 – 43, doi:http://dx.doi.org/10.5670/oceanog.2014.66, 2014.

Murray, R. J.: Explicit Generation of Orthogonal Grids for Ocean Models, Journal of Computational Physics, 126, 251 – 273, doi:http://dx.doi.org/10.1006/jcph.1996.0136, http://www.sciencedirect.com/science/article/pii/S0021999196901369, 1996.

Murray, R. J. and Reason, C.: A Curvilinear Version of the Bryan-Cox-Semtner Ocean Model and Its Representation of the Arctic Circulation, Journal of Computational Physics, 171, 1 – 46, doi:http://dx.doi.org/10.1006/jcph.2001.6761, http://www.sciencedirect.com/science/article/pii/S0021999101967610, 2001.

Nehari, Z.: Conformal mapping, Dover Publications, Inc., New York, reprinting of the 1952 edition, 1975.

Pain, C., Piggott, M., Goddard, A., Fang, F., Gorman, G., Marshall, D., Eaton, M., Power, P., and de Oliveira, C.: Three-dimensional unstructured mesh ocean modelling, Ocean Modelling, 10, 5 – 33, doi:http://dx.doi.org/10.1016/j.ocemod.2004.07.005, http://www.sciencedirect.com/science/

article/pii/S146350030400054X, the Second International Workshop on Unstructured Mesh Numerical Modelling of Coastal, Shelf and Ocean Flows, 2005.

Ringler, T., Petersen, M., Higdon, R. L., Jacobsen, D., Jones, P. W., and Maltrud, M.: A multi-resolution approach to global ocean modeling, Ocean Modelling, 69, 211 – 232, doi:http://dx.doi.org/10.1016/j.ocemod.2013.04.010, http://www.sciencedirect.com/science/article/pii/S1463500313000760, 2013.

Roberts, J. L., Heil, P., Murray, R. J., Holloway, D. S., and Bindoff, N. L.: Pole relocation for an orthogonal grid: An analytic method, Ocean Modelling, 12, 16 – 31, doi:http://dx.doi.org/10.1016/j.ocemod.2005.03.004, http://www.sciencedirect.com/science/article/pii/S1463500305000338, 2006.

Scholz, P., Lohmann, G., Wang, Q., and Danilov, S.: Evaluation of a Finite-Element Sea-Ice Ocean Model (FESOM) set-up to study the interannual to decadal variability in the deep-water formation rates, Ocean Dynamics, 63, 347–370, doi:10.1007/s10236-012-0590-0, http://dx.doi.org/10.1007/s10236-012-0590-0, 2013.

Shchepetkin, A. F. and McWilliams, J. C.: The regional oceanic modeling system (ROMS): a split-explicit, free-surface, topography-following-coordinate oceanic model, Ocean Modelling, 9, 347 – 404, doi:http://dx.doi.org/10.1016/j.ocemod.2004.08.002, http://www.sciencedirect.com/science/article/pii/S1463500304000484, 2005.

Storkey, D., Blockley, E., Furner, R., Guiavarch, C., Lea, D., Martin, M., Barciela, R., Hines, A., Hyder, P., and Siddorn, J.: Forecasting the ocean state using NEMO: The new FOAM system, Journal of Operational Oceanography, 3, 3 – 15, 2010.

Wang, Q., Danilov, S., Sidorenko, D., Timmermann, R., Wekerle, C., Wang, X., Jung, T., and Schröter, J.: The Finite Element Sea Ice-Ocean Model (FESOM) v.1.4: formulation of an ocean general circulation model, Geoscientific Model Development, 7, 663–693, doi:10.5194/gmd-7-663-2014, http://www.geosci-model-dev.net/7/663/2014/, 2014.

Xu, F. and Oey, L.: The Origin of Along-Shelf Pressure Gradient in the Middle Atlantic Bight, Journal of Physical Oceanography, 41, 1720 – 1740, doi:http://dx.doi.org/10.1175/2011JPO4589.1, 2011.

Table 1. Statistics of the sample orthogonal curvilinear grids.

Grid	Type	Turning Latitude	Non Lat-Lon Portion
GX1	Dipolar	0° N	50 %
TX0.1	Tripolar	29° N	25.8 %

Table 2. Continental boundaries and slit information.

Continent	Polygon Vertices	Slit Type	Area Proportion
Eurasia	(48° N, 6° E), (47° N, 14° E), (42° N, 21° E), (40° N, 30° E), (29° N, 55° E), (27° N, 60° E), (26° N, 69° E), (23° N, 73° E), (18° N, 75° E), (18° N, 80° E), (25° N, 90° E), (25° N, 92° E), (19° N, 96° E), (18° N, 98° E), (18° N, 104° E), (22° N, 107° E), (22° N, 110° E), (24° N, 116° E), (27° N, 119° E), (30° N, 120° E), (36° N, 118° E), (40° N, 116° E), (43° N, 122° E), (42° N, 125° E), (46° N, 134° E), (51° N, 136° E), (55° N, 132° E), (59° N, 138° E), (61° N, 143° E), (61° N, 152° E), (65° N, 170° E), (70° N, 145° E), (69° N, 120° E), (73° N, 95° E), (65° N, 80° E), (66° N, 55° E), (62° N, 40° E), (55° N, 25° E)	Circular	65.44 %
Africa	Northern Part: (31° N, 5° W), (25° N, 11° W), (14° N, 14° W), (8° N, 9° W), (8° N, 5° E), (5° N, 11° E), (0° N, 41° E), (8° N, 48° E), (10° N, 42° E), (17° N, 37° E), (29° N, 31° E), (31° N, 23° E), (29° N, 19° E), (32° N, 11° E), (35° N, 8° E), (34° N, 1° E) Southern Part: (17° S, 13° E), (23° S, 16° E), (28° S, 18° E), (31° S, 22° E), (30° S, 28° E), (23° S, 33° E), (18° S, 34° E), (15° S, 39° E), (10° S, 37° E), (5° S, 20° E), (10° S, 15° E), (12° S, 15° E)	Northern Part: Circular Southern Part: Radial	66.05 %
North-America	(54° N, 68° W), (50° N, 78° W), (50° N, 82° W), (57° N, 98° W), (65° N, 100° W), (66° N, 105° W), (66° N, 110° W), (68° N, 122° W), (68° N, 140° W), (67° N, 155° W), (65° N, 156° W), (63° N, 150° W), (62° N, 140° W), (52° N, 124° W), (49° N, 120° W), (45° N, 122° W), (39° N, 122° W), (35° N, 119° W), (32° N, 113° W), (25° N, 105° W), (25° N, 102° W), (31° N, 97° W), (32° N, 84° W), (36° N, 79° W), (39° N, 79° W), (44° N, 74° W)	Circular	56.55 %
South-America	(6° S, 39° W), (3° S, 48° W), (3° S, 52° W), (2° N, 55° W), (7° N, 64° W), (8° N, 74° W), (1.5° N, 75° W), (5° S, 78° W), (11° S, 74° W), (17° S, 68° W), (25° S, 68° W), (31° S, 68° W), (40° S, 71° W), (37° S, 63° W), (32° S, 61° W), (31° S, 54° W), (22° S, 49° W), (18° S, 43° W)	Radial	64.42 %

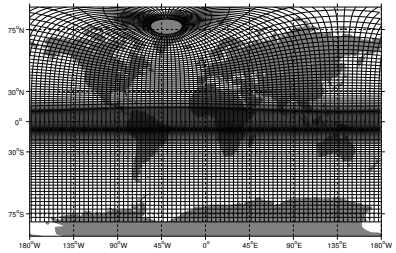

(a) Sample dipolar grid (GX1)

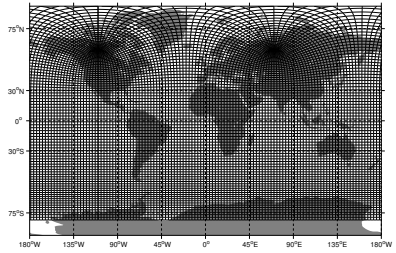

(b) Sample tripolar grid (TX0.1)

Figure 1. Orthogonal curvilinear grids for OGCMs.

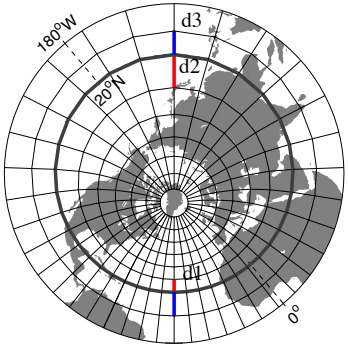

Figure 2. Northern patch constructed from a Moebius transformation.

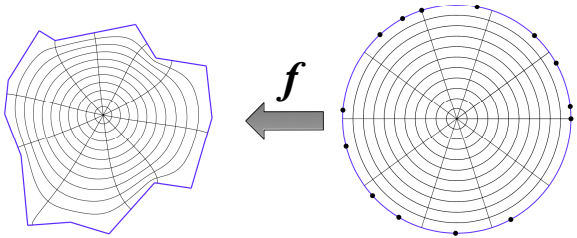

Figure 3. Schwarz–Christoffel mapping for single-connected polygon.

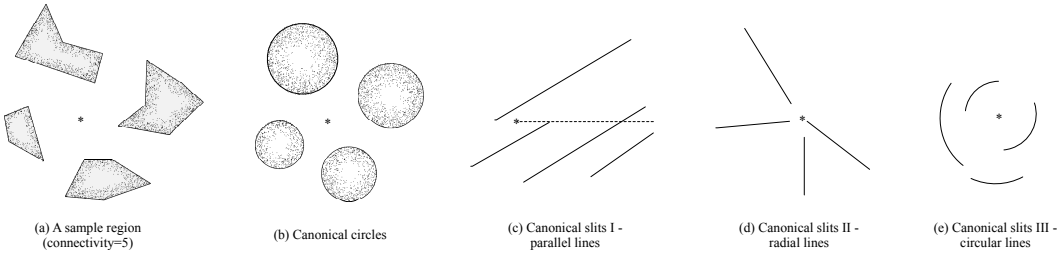

Figure 4. Multiply connected regions and canonical forms.

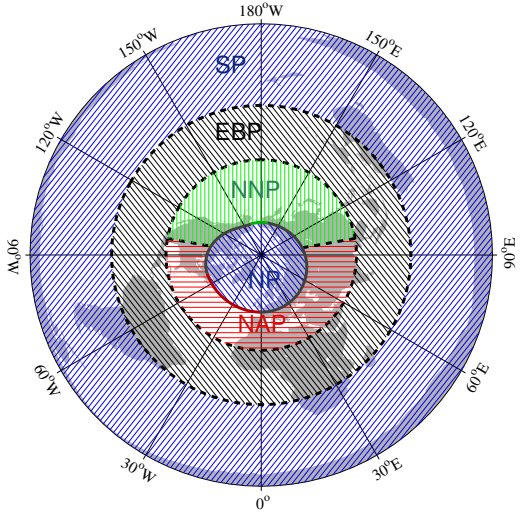

Figure 5. Patching scheme for the global grid.

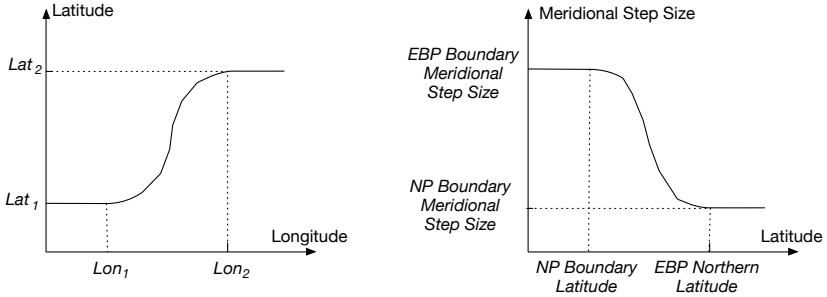

(a) Smooth linkage in NP boundary

(b) Meridional step size mitigation in NPP/NAP

Figure 6. Smooth linkage of NP boundary and meridional step size mitigation.

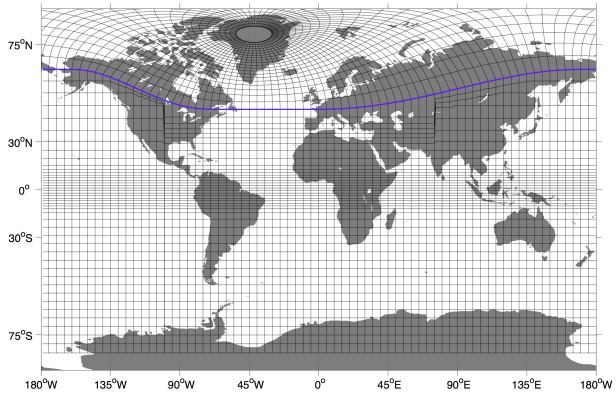

(a) Global grid

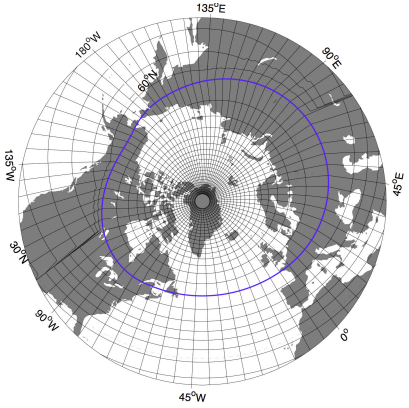

(b) North Polar part

Figure 7. Sample grid with nominal 1° resolution.

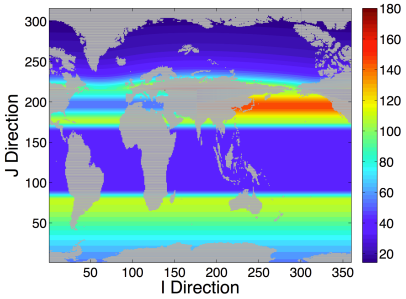

(a) Meridional step sizes (km)

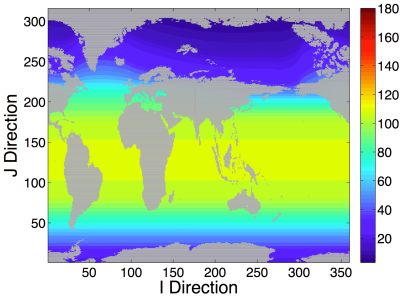

(b) Zonal step sizes (km)

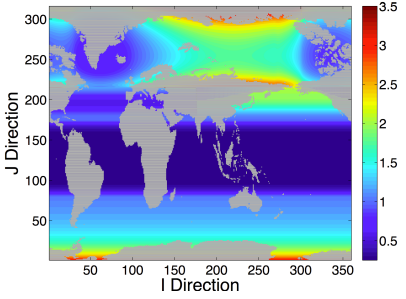

(c) Grid anisotropy

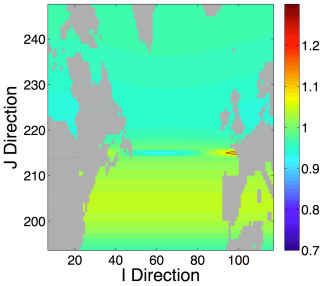

(d) Meridional scaling factor

Figure 8. Scales of 1° global grid with North Pole relocation.

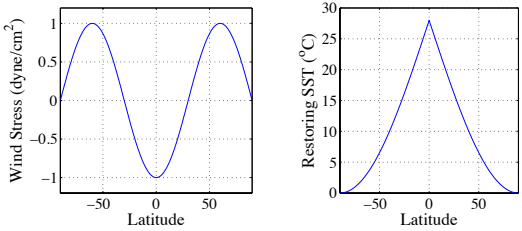

(a) Wind Stress Forcing (b) SST Restoring

Figure 9. Analytical wind stress and surface heat forcing.

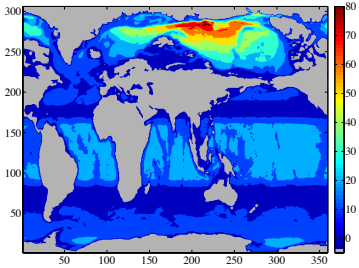

(a) Time step count per simulation hour

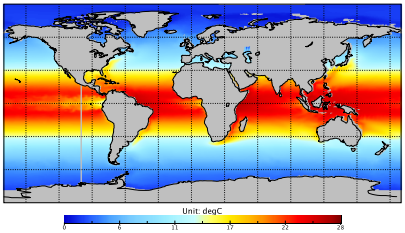

(b) Monthly mean SST field

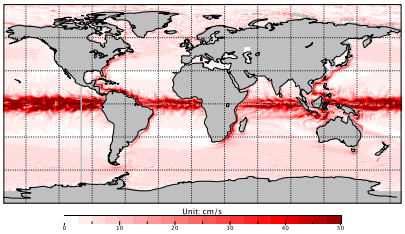

(c) Snapshot of surface velocity

Figure 10. Model evaluation of sample grid with SCSC mapping.

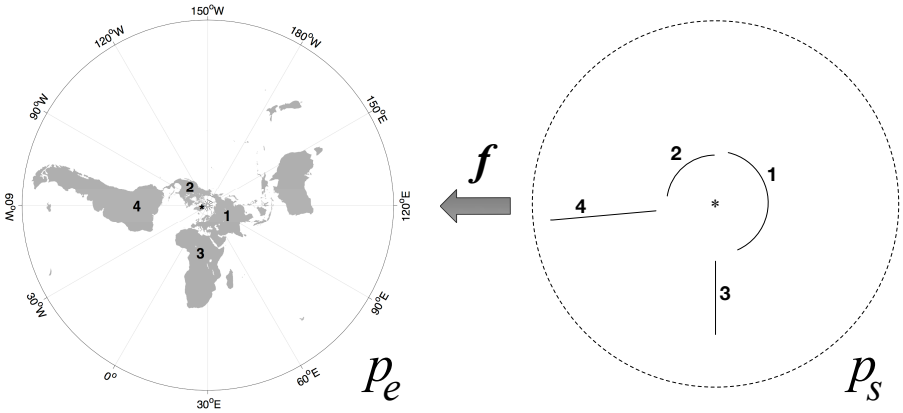

Figure 11. Conformal mapping between p_e and p_s.

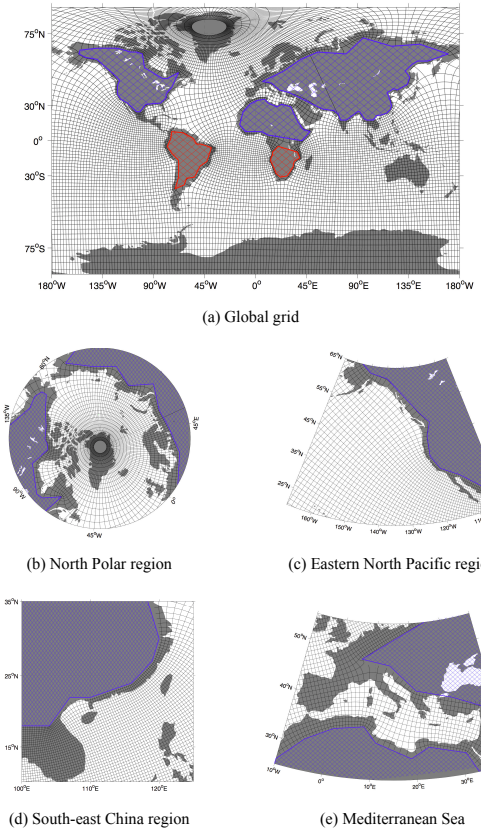

Figure 12. Global grid with MCSC mapping.

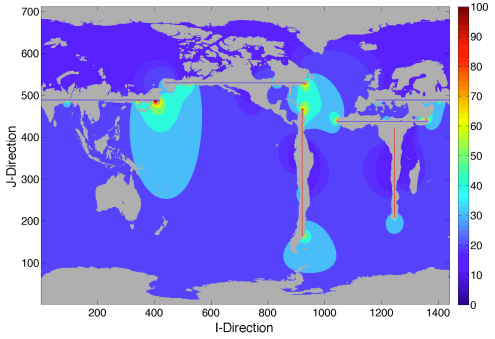

(a) Meridional step sizes

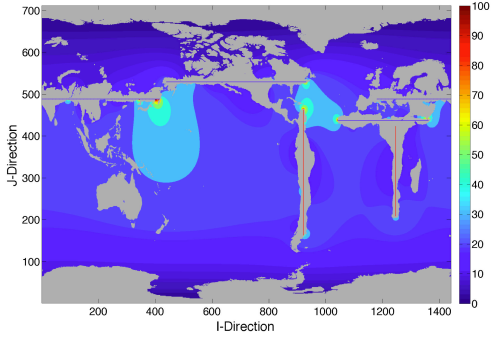

(b) Zonal step sizes

Figure 13. Meridional and zonal grid step sizes in grid space.

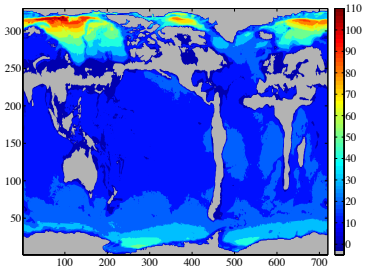

(a) Time step count per simulation hour

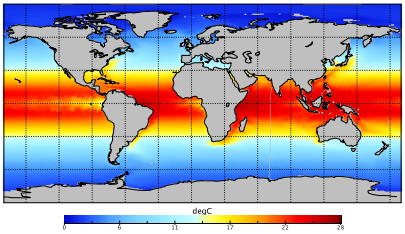

(b) Monthly mean SST field

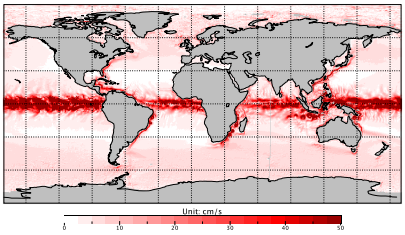

(c) Snapshot of surface velocity

Figure 14. Model evaluation of sample grid with MCSC mapping.